Undulation Instability of the Interface Between a Smectic-C Liquid Crystal and its Isotropic or Nematic Melt

J. Fournier, P. Galatola

J. Phys II France 5 (1995) 1297–1320 SEPTEMBER 1995, PAGE 1297

Classification
Physics Abstracts
61 30-v — 64 70Md — 68 10-m

Undulation Instability of the Interface Between a Smectic-C Liquid Crystal and its Isotropic or Nematic Melt

J.B. Fournier and P Galatola (*)

Laboratoire de Physique des Solides, Université Paris-Sud, Bâtiment 510, 91405 Orsay, France

(Received 22 February 1995, revised 18 May 1995, accepted 12 June 1995)

Abstract. — The spontaneous undulation instability of phase boundaries of smectics C is investigated both theoretically and experimentally. The driving mechanism is more efficient than that of Herring's instability of crystal surfaces, due to the coupling of a periodic distortion of the c-director with the interfacial undulation. The instability is studied experimentally in various geometries: free drops, capillaries and sandwiched cells. In the presence of a thermal gradient G, the undulation period is shown to scale as $G^{-1/3}$, as predicted theoretically. The existence of a threshold reflattening the interface in the presence of strong thermal gradients is investigated Upon varying the thickness of the smectic, a sequence of instabilities occurs which produces first the interfacial undulations, then focal conic defects as in the textural instability of the smectic-A–isotropic interface In free drops, the undulation instability yields a richer phenomenology arborescent patterns, splayed islands, spirals, trefoils, and eventually rows and triangular networks of focal conics.

1. Introduction

Patterns at phase boundaries are generally produced by some action exerted on the surface [1]. A typical example is directional solidification, i.e., a solid-liquid interface propagating at constant speed in a thermal gradient parallel to the pulling direction [2–4]. Dynamical patterns are well documented in liquid crystals, where pulling speeds and thermal gradients are easily accessible parameters [5–7], and the abundance of phases introduces a richer phenomenology [8–12]. A different way to destabilize a flat interface is to apply a large nonhydrostatic stress, as in the Grinfeld instability [13–16]. In the case of liquid crystals, similar instabilities can be obtained by applying electric [17] or magnetic fields [18].

Static interfaces can also be intrinsically unstable, as in the Herring instability [19, 20] of crystals, yielding spontaneous "hill and valley" interfacial patterns. This instability develops only for surface orientations of negative surface stiffness, corresponding to "prohibited" directions in the Wulff construction [21, 22], which do not necessarily exist. Recently, a generalized Herring instability has been observed at phase boundaries of "soft" materials, such as

(*) On leave from Dipartimento di Fisica, Politecnico di Torino, Corso Duca degli Abruzzi 24, 10129 Torino, Italy

smectic-C liquid crystals [23]. The mechanism of this instability is particularly efficient due to the coupling of a periodic distortion of the c-director with the surface modulation: a rough smectic-C–isotropic interface parallel to the layering direction is always unstable [23]; this can be shown from a more fundamental point of view by introducing a generalized surface stiffness for soft materials, which in the latter case is always negative [24].

In this paper we describe in detail the smectic-C–isotropic and smectic-C–nematic undulation instabilities. In Section 2, we first discuss some equilibrium properties of the interface between a smectic-C and its isotropic melt. We then present a linear stability analysis of smectic-C–isotropic interfaces in presence of a stabilizing thermal gradient. By suitable approximations we recover the simplified model of reference [23]. The case of the smectic-C–nematic instability is then briefly discussed. In Section 3, we describe a number of experimental observations related to the undulation instability. Various geometries are presented, i.e., free droplets showing: undulation stripe patterns, spontaneously splayed smectic islands, focal conics, and "spirals;" side views in rectangular capillaries of undulated smectic-C–isotropic and smectic-C–nematic interfaces; finally smectic-C's in sandwiched cells submitted to a thermal gradient normal to the glass plates, thus showing undulation stripe patterns. The latter geometry allows us to determine precisely both the director texture and the dependence of the instability period versus the applied thermal gradient. A comparison with the theory is presented. Attempts to reflatten the smectic-C-isotropic interface by applying strong thermal gradients are discussed in relation with the theoretical model.

2. Theory

According to the Gibbs-Thomson law [25], phase boundaries of first-order transitions are in general shifted with respect to the transition isotherm T_0. The shift in temperature is proportional to the mean curvature $1/R$ of the interface and to the surface tension γ. In the case of crystals, in cylindrical geometries for simplicity, the surface tension depends on the angle θ of the interface with respect to the crystal axes. The relevant quantity for the Gibbs-Thomson relation is the "surface stiffness" $\tilde{\gamma} = \gamma(\theta) + \gamma''(\theta)$ [22] (with a prime indicating differentiation):

$$\frac{\tilde{\gamma}}{R} = \mathcal{L}\frac{T - T_0}{T_0}, \tag{2.1}$$

where T is the interface temperature and $\mathcal{L}$ the transition latent heat per unit volume. Equation (2.1) expresses the equilibrium between the Laplace pressure $\tilde{\gamma}/R$ and the condensation pressure. In a non-equilibrium state, their difference represents the total pressure Π acting on the interface.

An equilibrium interface is stable if any perturbation relaxes, i e., if the pressure acting on an arbitrary bulge satisfies $\Pi R \equiv \tilde{\gamma} - (T/T_0 - 1)\mathcal{L}R > 0$, R being the bulge radius. For small bulges, this condition is equivalent to $\tilde{\gamma} > 0$, which is the local stability criterion. Note that the interface can nevertheless be globally unstable, i.e., for large R's, as is well-known in germination theory. When Herring's criterion

$$\tilde{\gamma} < 0 \tag{2.2}$$

is satisfied, the interface is unstable for small enough bulge radii R, and spontaneously breaks into Herring's "hill and valley" profile, which eventually satisfies (2.1) with $\tilde{\gamma} > 0$.

Smectic-C liquid crystals consist of equidistant layers of molecules tilted by an angle χ with respect to the layer normal [26]. At a smectic-C–isotropic interface with cylindrical symmetry and fixed orientation of layers, the surface tension $\gamma(\theta, \phi)$ is a function of *two* independent

angles: the angle θ defining the orientation of the interface, and the azimuthal angle ϕ of the c-director, which is the projection of the molecules onto the smectic layers. The stability analysis of a flat interface must take into account the elastic energy associated with the gradients of ϕ. Since this energy is always positive, it has a stabilizing effect. Let us consider the most unstable situation, corresponding to small wavevectors, for which the elastic energy ($\propto q$ per unit surface) is negligible with respect to the surface energy. In this limit, the azimuthal angle ϕ will adjust itself in order to locally minimize the surface energy $\gamma(\theta, \phi)$ for each given θ. Thus ϕ will be a function of θ, i.e., $\phi = \phi_e(\theta)$, through the relation

$$\gamma_\phi(\theta, \phi_e(\theta)) = 0. \tag{2.3}$$

Consequently, for large bulges the smectic-C formally behaves as a crystal with surface energy

$$\Gamma(\theta) = \gamma(\theta, \phi_e(\theta)). \tag{2.4}$$

According to Herring's condition (2.2), the instability will occur for $\Gamma + \Gamma'' < 0$. By differentiating (2.3) with respect to θ we get $\mathrm{d}\phi_e/\mathrm{d}\theta = -\gamma_{\theta\phi}/\gamma_{\phi\phi}$, yielding the instability condition

$$\gamma + \gamma_{\theta\theta} - \frac{\gamma_{\theta\phi}^2}{\gamma_{\phi\phi}} < 0. \tag{2.5}$$

Since $\gamma_{\phi\phi}$ can be assumed to be positive (otherwise the interface is from the very beginning unstable with respect to its director texture), the latter instability condition is easier to fulfill than that of the crystal $\gamma + \gamma_{\theta\theta} < 0$. In particular, when the smectic layers are parallel to the interface, $\gamma_{\phi\phi}$ is zero for symmetry reasons, and the interface is always unstable (unless this orientation corresponds precisely to a local minimum of γ).

A more formal demonstration of (2.5), based on a generalized Gibbs-Thomson equation for soft matter will be derived elsewhere [24]. In the following we shall recover these results from a linear stability analysis, taking the role of a thermal gradient into account.

2.1. Linear Stability Analysis. — Phase boundaries can be produced by application of a thermal gradient. Since the presence of the latter inhibits the formation of large bulges, the reasoning leading to the instability condition (2.5) is no longer valid To study in more detail the instability of the smectic-C–isotropic interface, we shall perform a linear stability analysis.

Let us consider a planar smectic-C–isotropic interface, forced by a thermal gradient $G > 0$ to lie in the plane $z = 0$. We consider an arbitrary configuration in which the surface and the texture are distorted, but the layers remain parallel to a fixed direction. The latter hypothesis, which amounts to neglecting layer compression, will be justified in Section (3.1.4). For simplicity, we assume that the structure is translationally invariant in the y-direction (Fig. 1). We call θ the angle of the interface with respect to the x-axis. We assume that the texture is initially at equilibrium with respect to the flat interface $\theta = 0$, the c-director being parallel to the azimuthal direction ϕ_0 such that $\gamma_\phi(0, \phi_0) = 0$ and $\gamma_{\phi\phi}(0, \phi_0) \geq 0$. In the distorted state, the interfacial profile is $z = u(x)$ and the bulk director distortion $\phi(x, z) = \phi_0 + \varphi(x, z)$.

The total free energy of the system, assumed to be semi-infinite, can be written as

$$\mathcal{F} = \int \mathrm{d}x\, \gamma[\theta(x), \phi_s(x)] \left(1 + u'^2(x)\right)^{1/2} + \int \mathrm{d}x \int_{-\infty}^{u(x)} \mathrm{d}z \left(\frac{\mathcal{L}}{T_0} G z + \frac{1}{2} K \left[\nabla \varphi(x, z)\right]^2\right), \tag{2.6}$$

where $\phi_s(x) = \phi(x, u(x))$ is the surface molecular orientation. The first term of (2.6) is the surface contribution, the second one is the bulk contribution which contains the smectic

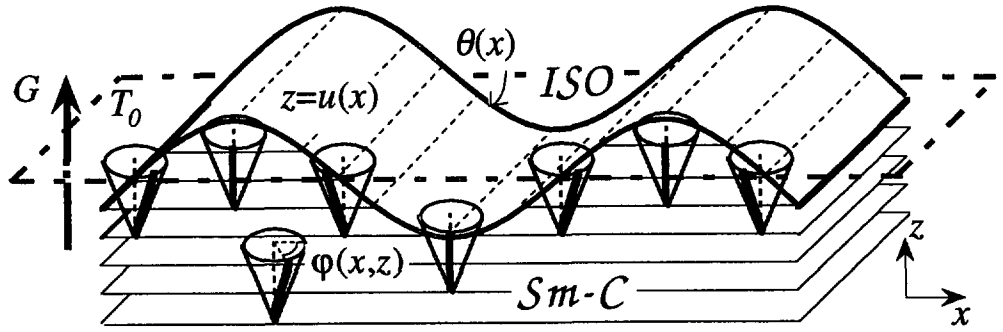

Fig. 1. — Interfacial distortions for studying the stability of a smectic-C–isotropic phase boundary For the sake of clarity, the layers are drawn parallel to the unperturbed interface. The picture represents the most unstable mode The main difference with Herring's instability of crystals is the possibility for the molecules to rotate on the cone within the layers to reduce the surface energy on the hill flanks of the profile: this greatly enhances the instability

condensation free energy density $\mathcal{L}(T(z) - T_0)/T_0$ and the c-director elastic energy density (in a one-constant approximation). The distortion free energy excess with respect to the flat profile ($u = 0$, $\phi = \phi_0$) is

$$\delta\mathcal{F} = \int \mathrm{d}x \left\{ \gamma[\theta(x), \phi_s(x)] \left(1 + u'^2(x)\right)^{1/2} - \gamma^{(0)} + \frac{\mathcal{L}}{2T_0} G u^2(x) \right\} + \int \mathrm{d}x \int_{-\infty}^{u(x)} \mathrm{d}z \, \frac{1}{2} K \left[\nabla\varphi(x,z)\right]^2 , \tag{2.7}$$

where $\gamma^{(0)} = \gamma(0, \phi_0)$. To check the stability of the flat interface, we expand (2.7) up to second order both in u and φ. Starting from

$$\theta(x) = u'(x) + O(3) \tag{2.8a}$$

$$\phi_s(x) = \phi_0 + \bar{\varphi}(x) + O(2), \tag{2.8b}$$

where $\bar{\varphi}(x) = \varphi(x, 0)$, we first develop

$$\gamma[\theta(x), \phi_s(x)] = \gamma^{(0)} + \gamma_\theta^{(0)} u'(x) + \frac{1}{2}\gamma_{\theta\theta}^{(0)} u'^2(x) + \frac{1}{2}\gamma_{\phi\phi}^{(0)} \bar{\varphi}^2(x) + \gamma_{\theta\varphi}^{(0)} u'(x)\bar{\varphi}(x) + O(3). \tag{2.9}$$

Using (2.9), we derive the second-order expansion of $\delta\mathcal{F}$:

$$\delta\mathcal{F}^{(2)} = \int \mathrm{d}x \left[\frac{1}{2}\tilde{\gamma}^{(0)} u'^2(x) + \frac{1}{2}\gamma_{\phi\phi}^{(0)} \bar{\varphi}^2(x) + \gamma_{\theta\varphi}^{(0)} u'(x)\bar{\varphi}(x) + \frac{\mathcal{L}}{2T_0} G u^2(x) \right] + \int \mathrm{d}x \int_{-\infty}^{0} \mathrm{d}z \, \frac{1}{2} K \left[\nabla\varphi(x,z)\right]^2 , \tag{2 10}$$

where we have set $\tilde{\gamma}^{(0)} = \gamma^{(0)} + \gamma_{\theta\theta}^{(0)}$.

Studying the stability of the flat interface is equivalent to studying the sign of (2.10) for arbitrary values of $u(x)$ and $\varphi(x,z)$. To do so, we perform a Fourier decomposition of $\delta\mathcal{F}^{(2)}$, assuming periodic boundary conditions along x in a box of length $2L$:

$$u(x) = \sum_q u_q e^{iqx} \tag{2.11a}$$

$$\bar{\varphi}(x) = \sum_q \bar{\varphi}_q e^{iqx}. \tag{2.11b}$$

Without loss of generality, the function $\varphi(x,z)$ can be chosen as the one $\varphi_e(x,z)$ minimizing the volumic integral in (2.10) for a given $\bar{\varphi}(x)$. indeed, if $\delta\mathcal{F}^{(2)}$ has negative values for a given set $\{u(x),\bar{\varphi}(x)\}$, then the flat interface is unstable; reciprocally, if it is always positive, $\delta\mathcal{F}^{(2)}$ is *a fortiori* positive for all functions $\varphi \neq \varphi_e$ and the flat interface is stable. The textures $\varphi_e(x,z)$ minimizing the volumic term in (2.10) are the solutions of $\Delta\varphi(x,z) = 0$ With the upper boundary condition $\varphi_e(x,0) = \bar{\varphi}(x)$, the solution is

$$\varphi_e(x,z) = \sum_q \bar{\varphi}_q e^{iqx} e^{qz} \tag{2.12}$$

By virtue of the relation $(\nabla\varphi)^2 = \mathrm{div}\,(\varphi\nabla\varphi) - \varphi\Delta\varphi$, the volumic integral in (2.10) can be reduced to a surface integral, since $\Delta\varphi = 0$:

$$\begin{aligned}\int_{-L}^{L} dx \int_{-\infty}^{0} dz \frac{1}{2} K \left[\nabla\varphi_e(x,z)\right]^2 &= \int_{-L}^{L} dx \frac{1}{2} K \bar{\varphi}(x) \varphi_z(x,0) \\ &= L \sum_q K|q||\bar{\varphi}_q|^2. \end{aligned} \tag{2.13}$$

Combining (2 10) and (2.13) we obtain, in Fourier components,

$$\begin{aligned}\delta\mathcal{F}^{(2)} = \quad & L \sum_q \left\{ \left(\tilde{\gamma}^{(0)} q^2 + \frac{\mathcal{L}}{T_0} G \right) |u_q|^2 + iq\gamma^{(0)}_{\theta\varphi} \left(u_q \bar{\varphi}^*_q - u^*_q \bar{\varphi}_q \right) \right. \\ & \left. + \left(K|q| + \gamma^{(0)}_{\phi\phi} \right) |\bar{\varphi}_q|^2 \right\}, \end{aligned} \tag{2.14}$$

or, diagonalizing,

$$\delta\mathcal{F}^{(2)} = L \sum_q \left\{ A(q) |u_q - i\alpha(q)\bar{\varphi}_q|^2 + B(q)|\bar{\varphi}_q|^2 \right\}, \tag{2.15}$$

with

$$A(q) = \tilde{\gamma}^{(0)} q^2 + \frac{\mathcal{L}}{T_0} G \tag{2.16a}$$

$$B(q) = K|q| + \gamma^{(0)}_{\phi\phi} - A^{-1}(q)\, q^2 \left(\gamma^{(0)}_{\theta\varphi} \right)^2 \tag{2.16b}$$

$$\alpha(q) = A^{-1}(q)\, q \gamma^{(0)}_{\theta\varphi}. \tag{2.16c}$$

As is clear from equation (2 15), the interface is unstable if, and only if, there exist q's such that $A(q) < 0$ or $B(q) < 0$.

2.1.1. General Case. — It follows from (2.16a) that $A(q)$ can be negative only if $\tilde{\gamma}^{(0)} < 0$. In this case, the interface is unstable whatever the thermal gradient, for large enough wavevectors. Conversely, when $\tilde{\gamma}^{(0)} > 0$, the interface can still be unstable, provided $B(q) < 0$. The most sensitive mode is then that which cancels the positive term proportional to $A(q)$, i.e., the *coupled* mode

$$u_q = \imath\alpha(q)\bar{\varphi}_q, \tag{2.17}$$

in which both the interface and the texture become unstable, one in quadrature with respect to the other (cf. Fig. 1). The condition $B(q) < 0$ is equivalent to

$$K\tilde{\gamma}^{(0)}|q|^3 + \left[\tilde{\gamma}^{(0)}\gamma_{\phi\phi}^{(0)} - \left(\gamma_{\theta\phi}^{(0)}\right)^2\right] q^2 + \frac{K\mathcal{L}G}{T_0}|q| + \frac{\mathcal{L}G}{T_0}\gamma_{\phi\phi}^{(0)} < 0. \tag{2.18}$$

In the above polynomial in $|q|$ all the coefficients are always positive but that of second order. Thus a necessary condition for the instability is

$$\tilde{\gamma}^{(0)}\gamma_{\phi\phi}^{(0)} - \left(\gamma_{\theta\phi}^{(0)}\right)^2 < 0, \tag{2.19}$$

which coincides with condition (2.5). If the latter is satisfied, there exists a threshold thermal gradient G_{th} below which the interface is unstable in a range of $|q|$: the interface is stabilized at small wavevectors by the thermal gradient, and at large wavevectors by the c-director elasticity. In particular, for $G = 0$ the interface is always unstable for small enough wavevectors, in agreement with the analysis presented at the beginning of this Section. Above G_{th} the interface is stable.

2.1.2. Degenerate Case. — Let us now consider the case of an interface parallel to the smectic layers, which corresponds to the most unstable situation. Indeed $\gamma_{\phi\phi}^{(0)}$ is zero by symmetry and condition (2.19) collapses to $-(\gamma_{\theta\phi}^{(0)})^2 < 0$, which is always satisfied In this case (2.18) simplifies, and trivial calculations yield

$$G_{\text{th}} = \frac{\left(\gamma_{\theta\varphi}^{(0)}\right)^4 T_0}{4K^2\tilde{\gamma}^{(0)}\mathcal{L}}. \tag{2.20}$$

At threshold, only one wavevector is unstable

$$q_{\text{th}} = \frac{\left(\gamma_{\theta\varphi}^{(0)}\right)^2}{2K\tilde{\gamma}^{(0)}}, \tag{2.21}$$

which is of the order of the characteristic wavevector of liquid-crystal patterns governed by a competition between surface tension and bulk elasticity [27, 28].

To conclude, a planar smectic-C–isotropic interface parallel to the layering direction is *always unstable*, unless this very orientation corresponds to a local minimum of the surface energy. It can be restabilized by a strong enough thermal gradient (cf. Fig. 2). Note that our analysis, limited to quadratic terms, does not allow us to discuss the order of the instability. One cannot exclude the possible existence of a first-order transition for $G > G_{\text{th}}$.

2.2. SIMPLIFIED MODEL. — In principle, higher-order terms in the free energy (2.14) would be necessary to determine the amplitude of the interfacial distortions. Nevertheless, for a well-developed instability, the amplitude of the surface profile can be estimated only from the

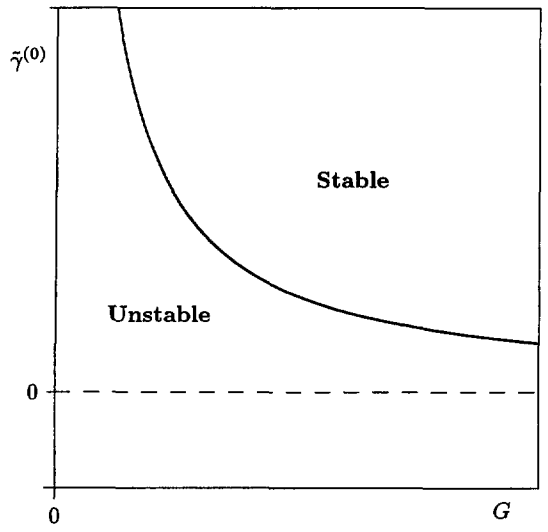

Fig. 2. — Stability diagram of a smectic-C phase boundary G is the thermal gradient applied normally to the interface and $\tilde{\gamma}^{(0)}$ is the usual surface stiffness as defined for crystals In the case of Herring's instability of crystals, only the region $\tilde{\gamma}^{(0)} < 0$ is unstable.

quadratic terms, by considering that the c-director distortion is saturated. Taking then for simplicity only one mode of amplitude $u_q = u$, with $\bar{\varphi}_q \sim 1$ the free energy (2.15) reduces to

$$\delta\mathcal{F}^{(2)}(u,q) \sim L\left\{A(q)|u - i\alpha(q)|^2 + B(q)\right\}. \tag{2.22}$$

For $\tilde{\gamma}^{(0)} > 0$, $A(q)$ is positive, and the minimum of (2.22) is obtained for $u = i\alpha(q)$, i.e., for the most unstable mode, with the q that minimizes $B(q)$. Solving the latter two equations yields, in the limit of small thermal gradients ($G \to 0$),

$$q \sim 2^{1/3}\left|\frac{\gamma^{(0)}_{\theta\varphi}}{\tilde{\gamma}^{(0)}}\right|^{2/3}\ell^{-1}, \tag{2.23a}$$

$$|u| \sim \left|\frac{\gamma^{(0)}_{\theta\varphi}}{2\tilde{\gamma}^{(0)}}\right|^{1/3}\ell, \tag{2.23b}$$

where there appears the characteristic length $\ell = (KT_0/\mathcal{L})^{1/3}G^{-1/3}$ over which the elastic energy density $\sim K/\ell^2$ compares with the condensation one $\sim (\mathcal{L}/T_0)G\ell$. But for numerical factors of order unity, we recover the results of the simplified model of reference [23].

2.3. Case of a Smectic-C–Nematic Interface. — If the smectic-C melt is a nematic phase, the interfacial energy γ should in principle depend on two additional angles specifying the orientation of the nematic director at the interface. We may however conjecture that the interfacial energy that a nematic distorsion could relax within the interface would be rather small compared to the total interfacial energy and therefore that the nematic director at the

interface should be almost continuous. In this case, the above mentioned additional variables are useless, and the problem is very similar to that of the smectic-C–isotropic interface. In the linear stability analysis of Section 2.1, the only difference is that the elastic energy within the nematic melt must also be considered. Without going into details, we may therefore consider that our theory applies equally well to the smectic-C–nematic interface, by simply assuming a somewhat larger value of the elastic constant K.

3. Experimental

We have studied the undulation instability of the smectic-C–isotropic interface in various geometries. The simplest way to create a smectic-C–isotropic interface is to deposit a liquid crystal droplet on a substrate, heated slightly above the smectic-C–isotropic transition, in order that a smectic cap appears on top of the drop. This naturally orients the smectic layers parallel to the interface, and thus always induces the instability. This geometry also allows us to study by Michelson interferometry the reaction of the instability on the free surface of the drop. The disadvantages of this method are the difficulty to control the thermal gradient, the presence of convection within the drop and a rather rapid evaporation of the liquid crystal.

Direct observation of the shape of the smectic-C–isotropic interface can be achieved in a capillary subjected to a thermal gradient. This experiment straightforwardly shows the undulation of the interface [23] It is however not convenient to study the director texture. The latter can be investigated in a sandwiched cell subjected to a thermal gradient orthogonal to the glass plates. This geometry allows for a good control of the anchoring conditions and of the thermal gradient, and is best to check the theoretical predictions of Section 2.

Most of the observations have been performed using the liquid crystal 4-n-hexadecyl-oxybenzoic acid, which presents a first-order smectic-C–isotropic transition at $\sim$ 135 °C [29]. Its main advantage consists in the rather large tilt angle, estimated here from birefringence measurements to be $\sim 45°$. The instability was also observed on the compound N, N'-Terephtalylidene-bis-[4-n-nonadecylaniline], displaying the same transition at the higher temperature of $\sim$ 150 °C. Lower temperature compounds, such as 4-n-tetradecyloxyphenil-4'-n-decylbenzoate and 4-n-decyloxyphenyl-4'-n-dodecyloxybenzoate, have also been investigated. They display the same instability undulation, however with a less pronounced amplitude, probably because of smaller tilt angles. Finally, the same qualitative behaviour was also observed at the smectic-C–nematic interface of compound 4,4'-di-n-heptyloxy-azoxybenzene, whose transition temperature is $\sim$ 95 °C. If not otherwise stated, all the successive experiments refer to the 4-n-hexadecyloxybenzoic acid.

In all our observations, the onset time of the stripe patterns is below our resolution (one video frame). This characteristic time $\lesssim 20$ ms is compatible with the expected response times of liquid crystal textures under changing boundary conditions [26]. The stripes never relaxed during our observations, i.e., for a time on the order of one day. We can therefore consider them as static patterns.

3.1. Free Droplet. — Our experimental set-up consists in the following (Fig. 3). A silane-coated glass holder is placed on an oven regulated slightly above the smectic-C–isotropic transition. A liquid crystal drop with typical radius ~ 0.5 mm and height $\sim 50\,\mu$m is laid on the glass substrate. A simple teflon cover is placed well above the sample, to create a vertical thermal gradient of a few °C/cm. To prevent air convection, a covering glass plate is placed $\sim 150\,\mu$m above the top of the drop, using $\sim 200\,\mu$m mylar spacers. Observations are made with a Leitz polarizing microscope between cross polarizers. A video camera connected to a video recorder is attached to the microscope. Observation of low birefringence patterns can be

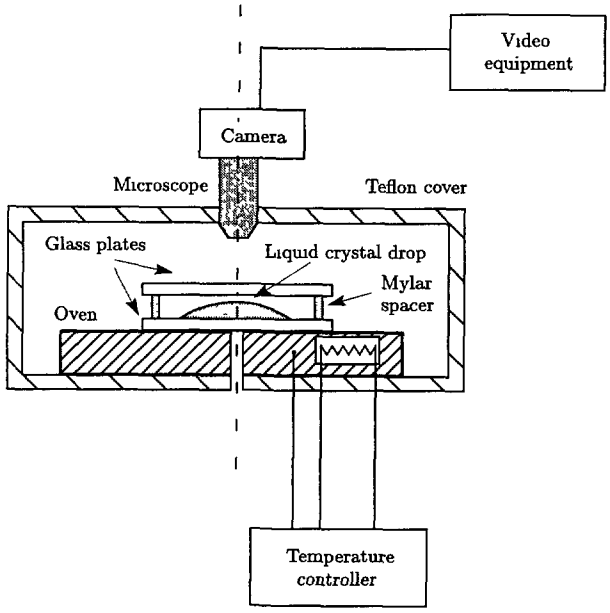

Fig 3 — Experimental set-up for the free drop geometry

performed by inserting a quarter-wave plate. Finally, the drop profile can be measured from equal-altitude fringes, using a Michelson interferometric lens (Ealing 25-0084).

3.1.1. Arborescent Patterns. — We start the experiment with the drop well in the isotropic phase. By suddenly cooling it down, we observe the appearance of a birefringent arborescent pattern (Fig. 4). With the quarter-wave plate at 45° with respect to the polarizers, the branches parallel to the polarizers appear as stripes longitudinally half black and half white. Those at 45° with respect to the polarizers appear as white bands on a black background, or the opposite. Between the branches, the liquid crystal remains grey as the surrounding isotropic phase.

By analogy with the usual wetting behaviour of smectics on free surfaces [30, 31], and in agreement with further observations, we assume that the smectic layers grow parallel to the smectic-air interface The alternance of black and white stripes within the branches corresponds then to a splay of the **c**-director, the latter being on average aligned parallel to the branches. Althought this is not clear at this stage, the formation of splayed arborescent structures is somehow linked with the surface undulation, as will be shown in the following

3.1.2. Smectic Islands. — Within somewhat larger drops, we observe the formation of elongated "smectic islands" with different sizes (Fig. 5). They are generated by a slow convection inside the isotropic phase that tears off pieces of the smectic cap. When the islands are oriented along the polarizers, they appear black at the center and white on the borders. By using a compensator, we determine that the islands bear a splay that spreads over their whole width, similarly to the branches of the arborescent patterns.

The existence of a **c**-director distortion splaying all over the width of the islands suggests an *anchoring* effect on their sides (Fig. 6). The "anchoring direction" being that of minimum

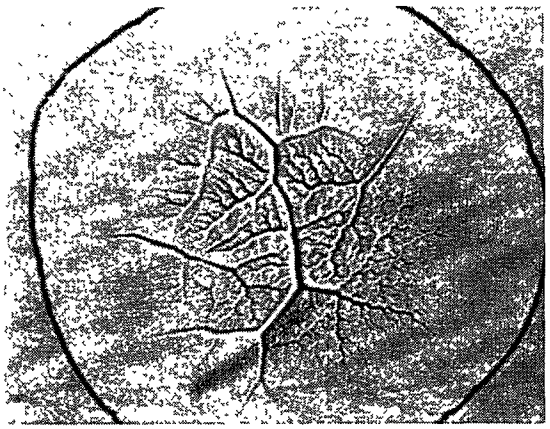

Fig. 4 — Arborescent pattern observed when an isotropic drop heated slightly above the smectic-C transition is suddenly cooled down Crossed polarizers parallel to the sides of the picture and quarter wave plate at 45° along the main diagonal. The diameter of the drop is $\sim 300\,\mu m$

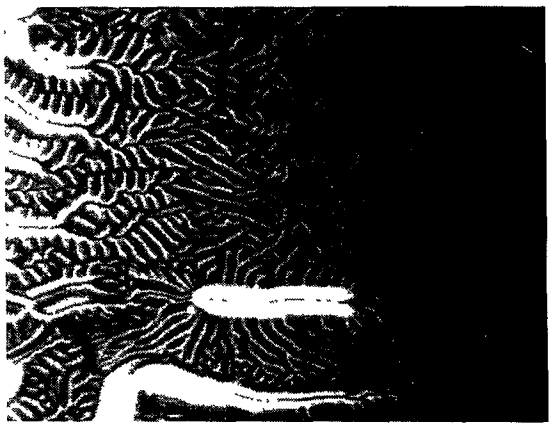

Fig 5. — Smectic-C "islands" floating at the top of an isotropic drop Crossed polarizers parallel to the sides of the picture and length of the isolated island $\sim 70\,\mu m$ The smectic layers are parallel to the free surface and a splay of the c-director extends over the whole width of the islands The branching between the islands is reminescent of the arborescent pattern of Figure 4.

energy for the function $\gamma(\theta, \phi)$, the observed splay is reminescent of the c-director distortion within the most unstable mode of the undulation instability, as described in Section 2.1.1. We may assume, by a rule of thumb, that the minimum energy orientation corresponds to the molecules parallel to the interface, by analogy with the properties of the smectic-A–isotropic interface [28, 32]. As for the above described splay within the branches, it is probably due to the same mechanism, although the branches themselves are likely to be of dynamical origin.

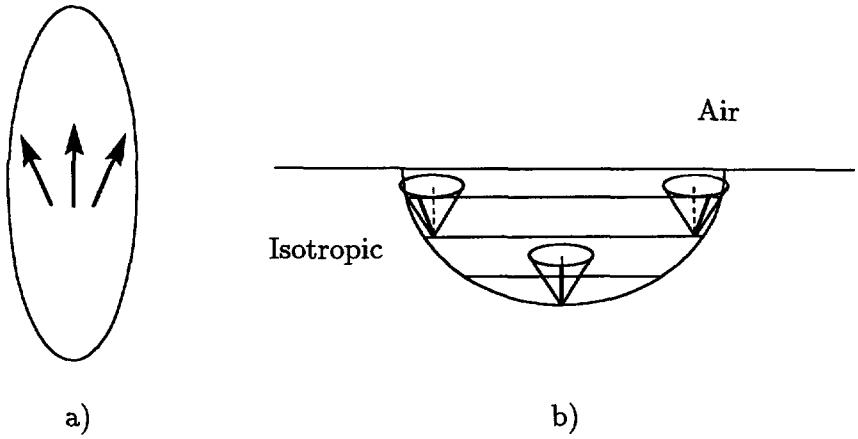

Fig 6. — Schematic representation of the spontaneous splay of the c-director within a smectic island, induced by the "anchoring" at the smectic-C–isotropic interface. a) Top view, b) Side view. Note the analogy with the most unstable mode of the undulation instability shown in Figure 1

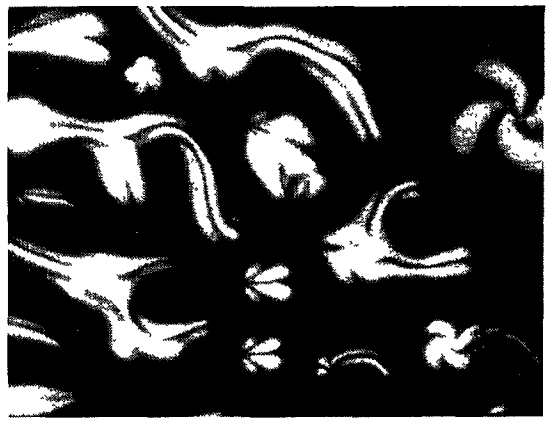

Fig. 7. — Islands transforming into "trefoils" and "spirals" Upper-right corner· a big right-handed spiral with diameter $\sim 50\,\mu$m. Lower-right corner. right-handed spirals with island-like tails On their left: two trefoils. Left side of the picture: branched islands Upper-left corner. a small left-handed spiral. Crossed polarizers parallel to the sides of the picture.

3.1.3. Spirals and Trefoils. — In elliptical islands with small aspect ratio, we observe a more or less radial splay with a +2 defect shifted with respect to the centre of the island. This *trefoil* texture (Fig 7) fits well with the assumed preferred parallel orientation of the molecules at the interface.

Elliptical islands generally take up a more circular shape while slowly melting. Then, sometimes, their texture suddenly undergoes a transition toward a chiral one. Such islands appear

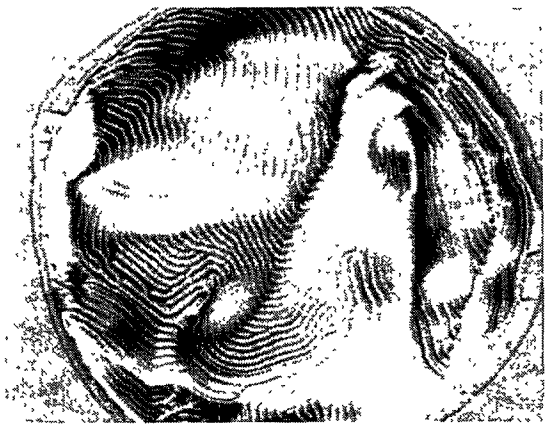

Fig. 8 — A free liquid crystal drop consisting of a smectic-C cap lying over a layer of isotropic phase. The phase coexistence is obtained by means of a vertical thermal gradient. The drop exhibits a stripe pattern of period $\sim 6\,\mu$m, revealing the undulation instability of the smectic-C–isotropic interface. Observation between crossed polarizers parallel to the sides of the picture with a quarter-wave plate at 45°.

between crossed polarizers as left or right-handed *spirals* (Fig. 7). Their texture can be explained as follows. When the sides of a circular island are sufficently abrupt, the angle between the interface normal and the layer normal can be larger than the smectic-C cone angle. There exist then two positions in which the molecules can be exactly parallel to the interface, symmetrical with respect to the radial direction. As the **c**-director assumes one of these directions on the borders of the island, a radial texture rotated with respect to the polarizers is generated. On the other hand, a pure radial texture is generated at the bottom of the drop, since the interface inclination there is generally less than the cone angle. The global texture resulting from the connection between these two regimes builds up a chiral pattern.

3.1.4. Periodic Stripe Patterns. — Stabilizing the smectic-C–isotropic interface at about half height of the drop, we observe a regular periodic pattern consisting of parallel stripes (Fig. 8). The corresponding texture is a periodic splay of the **c**-director, as shown when a compensator is used. A more detailed determination of the stripe texture has been performed in the sandwiched cell geometry. The presence of this pattern is in agreement with the undulation instability discussed in Section 2.

The compound undergoing the smectic-C–nematic transition also displays stripes in the same geometry (Fig 9). Observation of larger stripes shows the presence of disclination lines along the stripes, contrary to the smectic-C–isotropic case. The appearance of spontaneous distortions in smectic-C's was already reported in similar contexts [33–35]. As suggested in reference [23], it is likely that the presence of an undulating phase boundary had not been detected in these experiments; indeed, in all cases the smectic-C was in the vicinity of a nematic transition, as stated by the authors.

A basic assumption of our model (cf. Section 2.1) is that the smectic layers remain unperturbed, while it is the smectic-C–isotropic interface that undulates. To check this hypothesis, we have measured the shape of the free surface of the drop by using the Michelson interferometer. The equal altitude fringes displayed in Figure 10 reveal a free surface undulation of

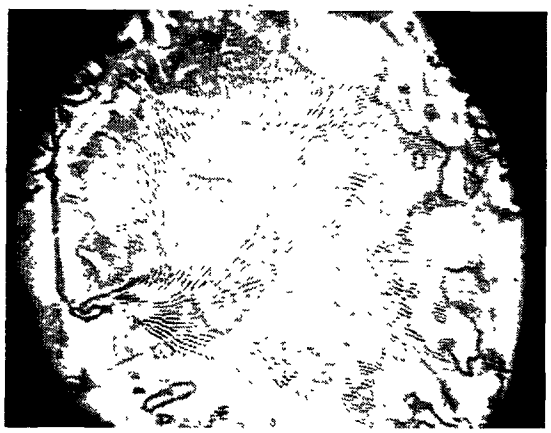

Fig. 9. — A free liquid crystal drop consisting of a smectic-C cap lying over a layer of nematic phase The stripe pattern shows the undulation instability of the smectic-C–nematic interface. The drop diameter is $\sim 500\,\mu$m. Observation between crossed polarizers parallel to the sides of the picture.

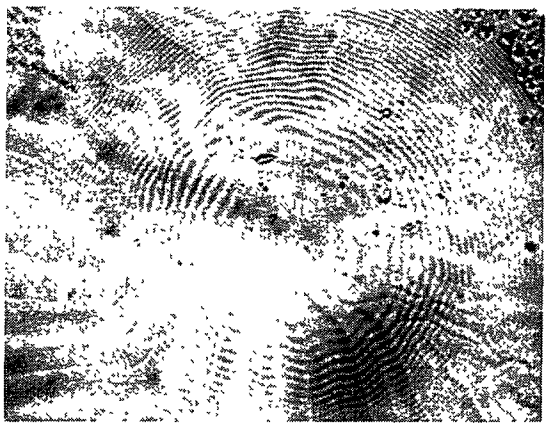

Fig. 10 — Image of the free surface of the smectic-C–isotropic drop. The undulation stripes are radial with period $\sim 15\,\mu$m. They are seen in transmission with a polarized white light The concentric pattern corresponds to equal altitude fringes obtained in reflection using a Michelson interferometer with a monochromatic green light. The fringes show a very weak undulation of the free surface of amplitude $\sim \pm 750$ Å, which assesses that the smectic layers remain almost flat while the smectic-C–isotropic interface undulates.

amplitude $\sim \pm 750$ Å correlated with a stripe pattern with period $\sim 15\,\mu$m for a smectic-C thickness $h \sim 30\,\mu$m. The free surface angle is $\sim 2 \times 10^{-2}$ rad, which is too small to be responsible for the observed birefringence modulation. If the instability would involve a layer undulation with amplitude A, instead of an interfacial undulation, the corresponding compression energy per unit surface E_B would be $\sim BA^2/h$, since the observed upper surface is flat on a macro-

Fig 11. — Rows of focal conics popping up along the stripes, with period $\sim 6\,\mu$m, of a smectic-C–isotropic free drop. This instability occurs above a thickness threshold of the smectic-C cap.

scopic scale. E_B must be compared with the elastic energy per unit surface of the c-director distortion $E_K \sim Kq^3A^2$. With $B \sim 2 \times 10^5\,\mathrm{erg/cm^3}$, $K \sim 10^{-6}\,\mathrm{erg/cm}$ [26], $2\pi/q = 15\,\mu$m, we get $E_B/E_K \sim 10^3$, which confirms that layer undulations can be neglected as they cost too much energy.

3.1 5. Focal Conics. — Above a threshold thickness of the smectic cap ~ 10–$20\,\mu$m, not well defined as in first-order transitions, rows of focal conics appear (Fig. 11). They progressively pop out one after another along the stripes, which they decorate as pearls. To determine the position of the focal conics with respect to the phase of the undulation, we slowly heat the drop again. The focal conics disappear, and the stripes eventually transform into smectic "fingers" separated by the isotropic phase. By continuity, we assess that the focal conics had appeared within the hollow part of the smectic in the undulation pattern.

Well above their onset thickness threshold, the focal conics fill up the whole space in a compact hexagonal network (Fig. 12a). Very large focal conics can be obtained in drops a few millimeters high, contained in a concave glass holder (Fig. 12b). They bear a disclination line, as topologically required in smectics-C [36–38], joining the revolution focal axis to the focal circle. Another thinner defect line, usually opposed to the previous one, is visible. It joins the revolution focal axis to a cusp defect of the focal circle, and could have the same origin as reported in reference [38].

The focal conic texture provides both a parallel orientation of the smectic layers at the upper free surface, and a perpendicular one at the lower isotropic interface. In smectic-A drop caps, a similar change in layer orientation, setting the molecules parallel to the isotropic interface, is responsible for an analogous instability [28]. Here, as can be shown by topological arguments, the presence of the main disclination line is compatible with a parallel orientation of the molecules at the isotropic interface, consistently with our model of the undulation mechanism.

In the smectic-C–nematic case, the thickness threshold for the appearance of focal conics is larger ~ 30–$50\,\mu$m. Above threshold, focal conic rows also appear within the stripes (Fig 13) and progessively fill up the whole drop in a hexagonal network.

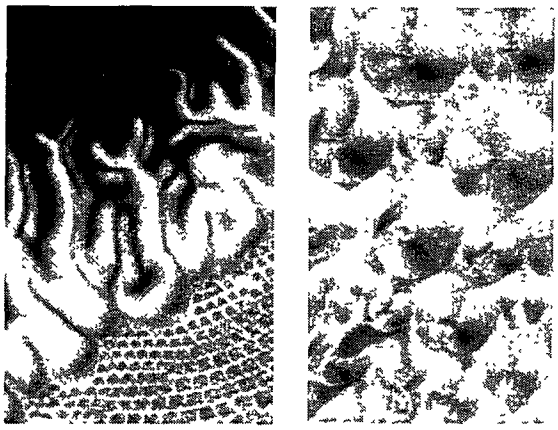

Fig. 12 — Thick smectic-C caps on top of isotropic drops The picture shows focal conics filling up the whole cap in a dense network that erases the stripe pattern a) Summary picture showing arborescent undulation stripes inside the isotropic phase connecting to a focal conic network as the smectic thickness increases; b) Very large focal conics with diameter $\sim 40\,\mu$m in a few millimeters high drop inside a concave glass holder. Disclination lines of the c-director are visible within the focal conics

3.2. VIEWS OF THE INTERFACE. — In order to observe the profile of the smectic-C–isotropic interface, we use a glass capillary of rectangular section 0.1×1 mm. We submit it to a thermal gradient parallel to the 1 mm sides, obtained by contacting one of the vertical 0.1 mm sides of the capillary with a brass oven, and the opposite side with a brass plate insulated from the oven by a teflon spacer (Fig. 14). The capillary glass walls are untreated.

Varying the average temperature, we stabilize an interface between the smectic-C and its isotropic phase with the layers parallel to the interface. Observation under the microscope shows (Fig. 15a) a static interface undulation. The surface profile is not exactly sinusoidal: the thickness minima appear somewhat flatter than the maxima. The high birefringence of the smectic-C within the undulation shows that the latter is not a wetting artefact. With a typical thermal gradient $G \sim 0.5\,°\mathrm{C/cm}$, we observe a period $\sim 23\,\mu$m and an amplitude $\sim \pm 3.5\,\mu$m, corresponding to a maximum interface tilt $\sim 40\,°$. The undulations are usually stable for a few minutes, after which they drift under flow convection due to stray thermal gradients, probably due to thermal contact inhomogeneities along the capillary axis. Sometimes the undulations disappear, probably having rotated by $90\,°$.

In accordance with the observations in free droplets, when we increase the average thickness of the smectic-C, we observe the appearance of focal conics superimposed with the undulations (Fig. 15b). The focal conics appear in correspondence within the thickness minima; they are materialized by their disclination lines which go from the interface to the opposite capillary wall.

The same experiment with the smectic-C–nematic compound presents additional complica-

Fig 13 — Stripes displaying rows of focal conics in a thick smectic-C–nematic drop. The width of the stripes is $\sim 36\,\mu$m.

tions. The glass walls usually provide a favorable degenerate planar anchoring. Nevertheless, several defects are usually present, often induced by anchoring memory effects of the smectic layers. In the presence of a defect induced nematic texture, the smectic-C–nematic interface is hardly visible. Under good conditions, we do observe an undulation of the interface, which is different from the smectic-C–isotropic one (Fig. 16). In particular, it is likely the presence of disclination lines in the smectic-C thickness minima. With an estimated thermal gradient $G \sim 0.2\,°$C/cm, we observe a period $\sim 32\,\mu$m and an amplitude $\sim \pm 3.2\,\mu$m, corresponding to an interface tilt $\sim 22\,°$. We did not succeed in observing focal conics inside the undulations, due to the larger value of their onset thickness threshold.

3.3. Sandwiched Cell Geometry. — The experimental set-up is depicted in Figure 17 The sample consists in a cell made of two 1-mm-thick silane-coated glass plates to align the smectic layers parallel to the substrates. The glasses are separated by $\sim 50\,\mu$m mylar spacers. The gap is filled with the liquid crystal in its isotropic phase. A vertical gradient in the range ~ 0.5–$600\,°$C/cm, with a relative error better than 5%, is created by heating the sample from below with an electrical oven and from above by a circulation of siliconic oil. The sample is observed perpendicularly to the glass plates with a Leitz polarizing microscope.

3.3.1. Stripes Texture. — Adjusting the temperatures, a horizontal smectic-C–isotropic interface can be stabilized approximately in the middle of the cell. The smectic-C exhibits the same periodic striped texture as in the free drop (cf. Section 3.1.4) In order to study the director texture, we generate stripes with large width $\sim 20\,\mu$m by means of a low thermal gradient $\sim 0.5\,°$/cm (Fig. 18). The average smectic-C thickness is $\sim 10\,\mu$m.

With the polarizer P parallel to the stripes and the analyzer A crossed, we see alternate thin and thick black lines. The thin (resp. thick) lines correspond to the zones where the smectic is thicker (resp. thinner). Their width difference could be due to an asymmetry of the interface profile or to lens effects. Rotating P by $\pi/2$ at fixed A, the thin and thick lines merge together while black bands appear in between. Rotating A at fixed P, only the contrast changes, which indicates that the molecules close to the upper plate have a uniform orientation. We do not

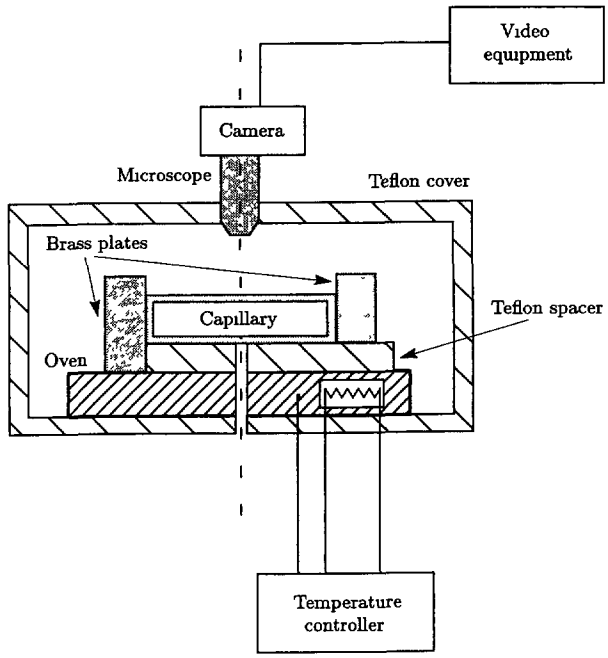

Fig 14 — Experimental set-up for the side-view observations in a glass capillary

observe any surface disclination. From these observations, we deduce the existence of a periodic twist through the sample thickness, relaxing a smooth periodic splay of the c-director at the smectic-C–isotropic interface. The relatively large birefringence ($\sim 0\,1$) allows us to apply the Mauguin criterion [26]: the optical and the molecular twist are equal. Thus, at the isotropic interface the c-director is parallel to the stripes where the thickness is minimum or maximum, and splays by $\pi/2$ in between.

Using the compound undergoing the smectic-C–nematic transition, we also observe (Fig. 19) stripe patterns similar to those appearing in the free drop geometry (cf. Section 3.1.4). The determination of their texture is however more delicate due to the underlying nematic phase.

In both cases, when the smectic-C thickness is large enough, rows of focal conics appear within the stripes, displaying the same behaviour as previoulsy described.

3.3.2. Period Measurements. — Measurements of the period of the stripe pattern as a function of the applied thermal gradient have been performed both for smectic-C–isotropic and smectic-C–nematic interfaces [23]. The results, shown in Figure 20, reveal a power law with exponent -0.33 ± 0.04, in good agreement with the theoretical prediction (cf. Section 2.2). The range of thermal gradients ~ 3–$400\,°C/cm$ is limited above by the onset of convection, and below by the nucleation of "bâtonnets" [39].

According to equation (2.23a), the asymptotic period, in the limit of low thermal gradients, is $\lambda = \beta G^{-1/3}$ with

$$\beta = \pi(2\tilde{\gamma}^{(0)}/\gamma_{\theta\phi}^{(0)})^{2/3}\,(KT_0/\mathcal{L})^{1/3} \tag{3.1}$$

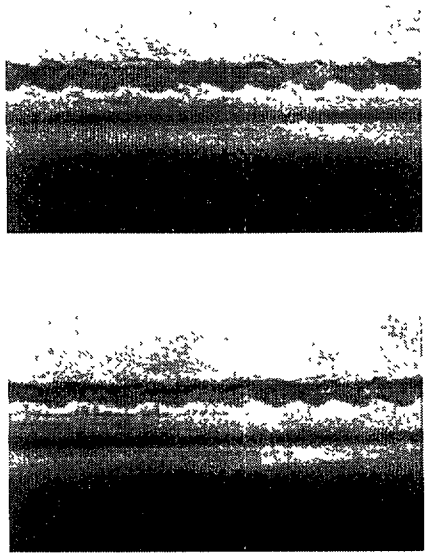

Fig 15 — Side views of the undulating smectic-C–isotropic interface in a glass capillary (as in Ref. [23]). The smectic-C is on the lower part of the image, in contact with the coldest side of the capillary (black in the picture), which touches the right brass plate in Figure 14 The undulations have period $\sim 23\,\mu$m and amplitude $\sim \pm 3\,5\,\mu$m. a) Average thickness of the smectic-C plate $h \sim 10\,\mu$m; b) $h \sim 15\,\mu$m· focal conics connect the capillary glass to the interface points of smectic-C thinner thickness.

Within the error bars, for both compounds, we obtain $\beta \sim 15.4 \times 10^{-4}$ cgs. For the smectic-C–isotropic interface, assuming $K \sim 10^{-6}$ dyn, and with $\mathcal{L}/T_0 \sim 6.5 \times 10^5$ cgs [23], we estimate $\gamma_{\theta\phi}^{(0)}/\tilde{\gamma}^{(0)} \sim 0.23$, in reasonable agreement with usual values of surface energy anisotropies in smectics in contact with their melt [28]. For the smectic-C–nematic interface, setting K twice as before to take into account the distortion energy inside the nematic phase, and with $\mathcal{L}/T_0 \sim 1.1 \times 10^5$ cgs [23], we get a somewhat larger ratio $\gamma_{\theta\phi}^{(0)}/\tilde{\gamma}^{(0)} \sim 0.78$.

3.3.3. Strong Gradients. — Our model predicts the existence of a thermal gradient threshold (2.20) above which the interface is stable or at least metastable (cf Section 2). Let us estimate $G_{\rm th}$ and the corresponding period $\lambda_{\rm th} = 2\pi/q_{\rm th}$ for the smectic-C–isotropic compound. We write equations (2.20) and (2 21) as

$$G_{\rm th} = \frac{1}{4}\frac{\gamma_{\theta\varphi}^{(0)}}{\tilde{\gamma}^{(0)}}\left(\frac{K}{\gamma_{\theta\varphi}^{(0)}}\right)^{-3}\left(\frac{\mathcal{L}}{T_0}\right)^{-1} K, \tag{3.2a}$$

$$\lambda_{\rm th} = 4\pi\left(\frac{\gamma_{\theta\varphi}^{(0)}}{\tilde{\gamma}^{(0)}}\right)^{-1}\frac{K}{\gamma_{\theta\varphi}^{(0)}}. \tag{3.2b}$$

With $K \sim 10^{-6}$ dyn, $\mathcal{L}/T_0 \sim 6.5 \times 10^5$ cgs [23], and $\gamma_{\theta\varphi}^{(0)}/\tilde{\gamma}^{(0)} \sim 0.23$ as previously estimated, the only unkown quantity is the characteristic length $K/\gamma_{\theta\varphi}^{(0)}$. In a Landau-like model of the

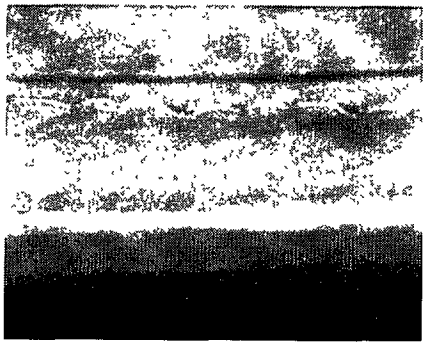

Fig. 16 — Side view of the undulating smectic-C–nematic interface in a glass capillary The smectic-C is on the lower part of the image, in contact with the shallow side of the capillary (black in the picture). The undulation period is $\sim 32\,\mu$m and the amplitude is $\sim \pm 3\,2\,\mu$m

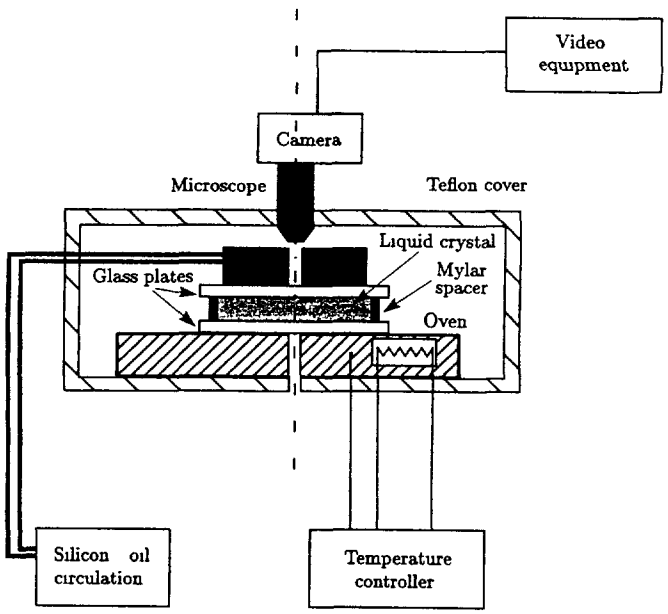

Fig. 17 — Experimental set-up for the sandwich cell geometry

interface [26], $K/\gamma^{(0)}$ is expected to compare with the coherence length $\xi \sim 100$ Å of the first-order smectic-C–isotropic transition. Since we estimated $\gamma^{(0)}_{\theta\varphi}/\tilde{\gamma}^{(0)} \sim 0.23$, it seems reasonable to take $K/\gamma^{(0)}_{\theta\varphi} \sim 400$ Å. With these values we obtain $G_{\rm th} \sim 1400\,^{\circ}$C/cm and $\lambda_{\rm th} \sim 2\,\mu$m.

With our experimental set-up, we were not able to reach thermal gradients higher than

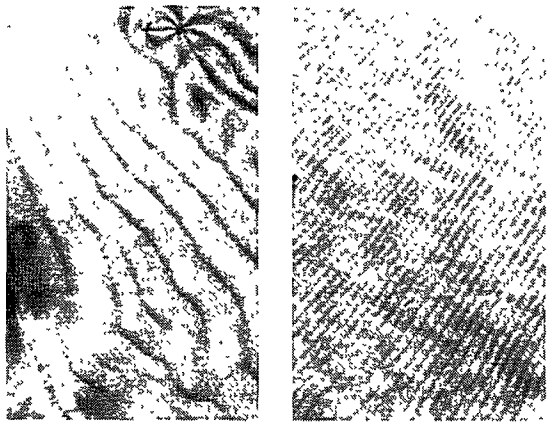

Fig. 18. — Undulation stripes of the smectic-C–isotropic interface in a cell submitted to a thermal gradient a) Low thermal gradient (0.5 °C/cm): large stripes with period $\sim 20\,\mu$m; b) Strong thermal gradient (60 °C/cm): small stripes with period $\sim 4\,\mu$m.

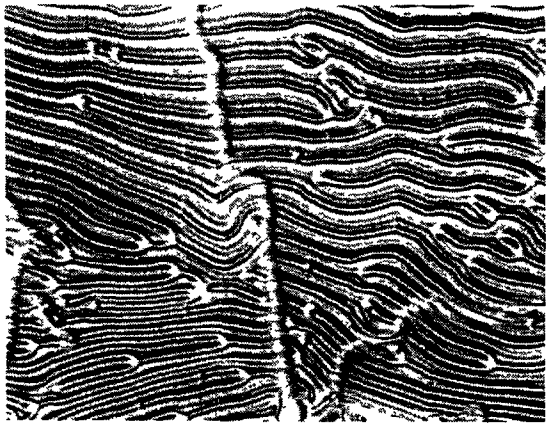

Fig. 19 — Undulation stripes of the smectic-C–nematic interface in a cell submitted to a 5 °C/cm thermal gradient. The period of the stripes is $\sim 9\,\mu$m.

~ 1000 °C/cm. To avoid convection due to stray thermal gradients, we switched to $\sim 6\,\mu$m thin cells; however, the presence of impurities and dust particles yielded thermal short circuits and a certain amount of thermal convection With $G \sim 1000$ °C/cm, we observed a saturation of the undulation period to a value at the limit of optical resolution, i.e., compatible with $\lambda_{th} \sim 2\,\mu$m. Actually, the presence of dust particles allowed us to observe simultaneously the

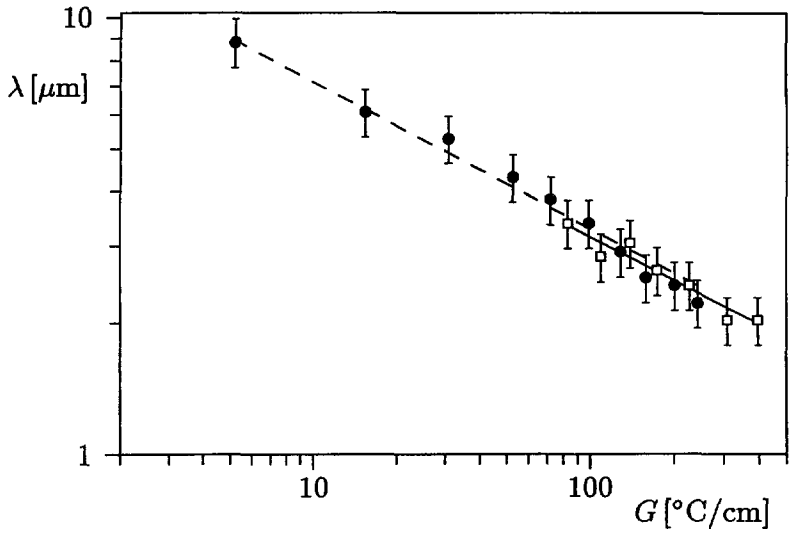

Fig. 20 — Log-log plot of the undulation period λ as a function of the applied thermal gradient G (as in Ref [23]) Open squares: smectic-C–isotropic interface in 4-*n*-hexadecyloxybenzoic acid; closed circles: smectic-C–nematic interface in 4,4'-di-*n*-heptyloxy-azoxybenzene. The best fit lines have a slope of −0.33

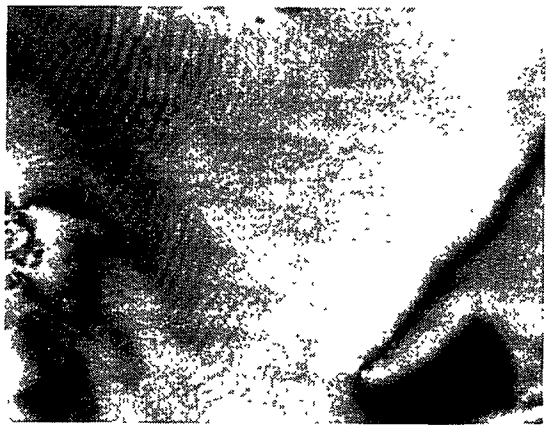

Fig. 21. — High and low thermal gradient regimes in a thin ($\sim 6\,\mu$m) cell. Close to the dust particle, convection lowers the thermal gradient and large periods are visible. Far from the dust particle the undulation instability is hardly visible.

high and the low thermal gradients regimes: close to the dust particles—where the convection lowers the thermal gradient—we observed large periods, whereas far from them the undulation instability was hardly visible (Fig. 21).

With the smectic-C–nematic compound, we observed qualitatively the same behaviour However, the thermal convection was larger, possibly due to the anisotropy of the nematic thermal

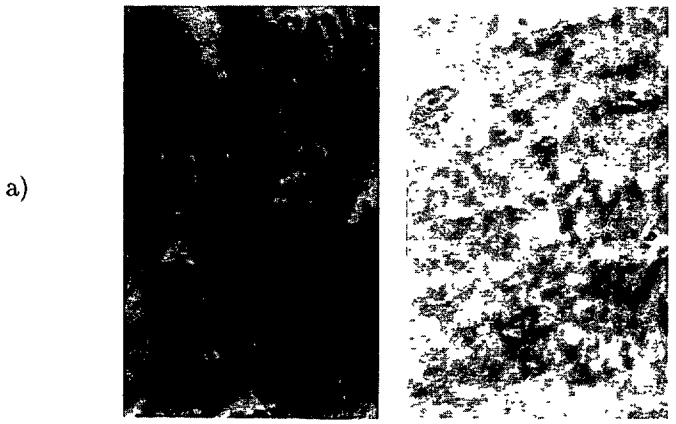

Fig. 22. — Textures observed in the sandwich cell geometry with the compound 4-*n*-decyloxyphenyl-4'-*n*-dodecyloxybenzoate, showing a smectic-C–isotropic transition at $\sim 90\,^{\circ}$C a) Periodic undulations with period $\sim 6\,\mu$m for a thermal gradient $\sim 50\,^{\circ}$C/cm; b) Absence of stripes for a thermal gradient $>$ 80 °C/cm. The thickness of the smectic-C is a few microns. A quarter wave plate is inserted between the cross polarizers to enhance the contrast.

conductivity [40,41].

In principle, lower threshold thermal gradients and larger threshold periods are expected in the case of smectic-C compounds with smaller tilt angle c. Indeed, assuming $K \propto c^2$ and $\gamma^{(0)}_{\theta\phi} \propto c^2$, we expect $G_{\rm th} \propto c^4$ and $\lambda_{\rm th} \propto c^{-2}$. We have therefore investigated the compounds 4-*n*-tetradecyloxyphenil-4'-*n*-decylbenzoate and 4-*n*-decyloxyphenyl-4'-*n*-dodecyloxybenzoate, having a tilt angle $c < 30°$. In practice, we had problems to properly orient the smectic layers, and observations were difficult due to focal conics usually appearing at very small thicknesses (a few μm). In one sample, however, we succeeded in obtaining regions with and without stripes, for gradients smaller and larger than $\sim 80°$C/cm, respectively (Fig. 22). It is however difficult to discuss this observation within our model, since the thickness of the smectic was smaller than the undulation period.

4. Conclusions

Our observations have shown that smectics-C in contact with their melt (isotropic or nematic) display a sequence of instabilities. For small thicknesses, the smectic-C exhibits a stripe pattern due to a *spontaneous undulation* of its interface, coupled to a periodic distortion of the c-director [23]. The smectic layers however remain flat. For larger thicknesses, circular focal conics, i.e., domains of curved equidistant layers, appear as rows inside the undulation stripes and eventually fill up the whole smectic.

The spontaneous undulation of the interface is reminiscent of the Herring instability in crystals [19]. According to our model, however, the coupling with the c-director texture greatly enhances the instability. In terms of the surface energy γ—depending on the angle θ between the interface and the smectic layers, and on the surface orientation ϕ of the c-director—, the instability condition reads $\gamma + \gamma_{\theta\theta} < \gamma^2_{\theta\phi}/\gamma_{\phi\phi}$ (with $\gamma_{\phi\phi} > 0$). When the smectic layers are parallel to the unperturbed interface, $\gamma_{\phi\phi} = 0$ and this condition is always satisfied, unless the interface orientation corresponds to a minimum of γ. In particular, the interface must be *rough* [22] to yield the instability, which seems to be the case experimentally. For an arbitrary

orientation of the smectic layers, the instability condition is easier to satisfy than the crystal condition $\gamma + \gamma_{\theta\theta} < 0$.

We have directly observed the undulations of the smectic-C–isotropic and smectic-C–nematic interfaces, and studied the corresponding instabilities in the presence of a stabilizing thermal gradient We found that the period of the undulation scales as $G^{-1/3}$ for small thermal gradients G, as predicted in our linearized model. In large stripes, we observed and measured a splay of the c-director parallel to the interface, and assessed the presence of a perpendicular twist relaxing the surface distortion, in agreement with the most unstable mode in our model. Finally, we have shown clues of the existence of a thermal gradient threshold above which a flat interface is stable or at least metastable, as theoretically predicted. A clear determination was not possible due to limitations in the reachable thermal gradients in our experimental apparatus ($\sim 1000\,°C/cm$).

Within our linearized model, we cannot determine precisely which orientation of the layer and c-director minimize the surface energies of the smectic-C–isotropic or smectic-C–nematic interfaces. We can only assess that the orientation corresponding to the layers parallel to the interface, with the molecules at the cone angle with respect to the interface, does *not* correspond to the minimum energy For the smectic-C–isotropic interface we had the feeling from the free drop experiment that the molecules preferentially orient parallel to the interface. This seems reasonable as it sets an equal amount of hydrophilic and hydrophobic groups in contact with the isotropic phase, which in average is neither hydrophilic nor hydrophobic, thus satisfying the usual segregation rule of amphiphiles. This reasoning however does not hold for the smectic-C–nematic interface, at which the nematic orientation is expected to be almost continuous. For the latter, the layer orientation is probably an important factor.

The second event in the instability cascade is the appearance of *focal conics*, as in the instability of the smectic-A–isotropic interface [28,32]. The presence of cylindrical focal conics provides both a parallel orientation of the layers at the upper material boundary (glass plate or drop free surface), and a *perpendicular* orientation of the layers at the smectic-C–melt interface. Due to the latter, the molecules have a larger choice of orientations, including the parallel one probably favored at the boundary with the isotropic phase. From an energetical point of view, focal conics involve only curvature distortions, which are easily accessible in smectics. As discussed in references [27,28], a focal conic with radius r implies an elastic energy $\propto r$, while it relaxes an interfacial energy $\propto r^2$. Focal conics are thus energetically favored at large r's, or equivalently for large enough smectic-C thicknesses. Eventually, focal conics provide the most efficient way to relax the anisotropic interfacial energy, as a large number of molecular interfacial orientations can be achieved without any undulation of the interface. Finally, the nucleation of rows of focal conics—within the hollow part of the smectic in the undulation pattern—is reminescent of the way focal conics appear on the dynamical undulations of rapidly growing smectic-A–isotropic interfaces [42]. As corroborated by the Michelson interferometer observations (cf. Section 3.1.4), the smectic layers are weakly bent in opposite directions where the focal conics subsequently appear, which is likely to induce pricking fractures, as described in reference [42].

Acknowledgments

This work has benefited from fruitful discussions with G. Durand. Thanks are also due to C. Germain for material synthesis, and to D. Guillon for providing the low temperature smectic-C–isotropic compounds. One of us (P.G.) was supported by an EEC Network Scholarship.

References

[1] See, for example, Pattern Formation in Complex Dissipative Systems, S Kai, Ed (World Scientific, Singapore, 1992).

[2] Mullins W.W. and Sekerka R F , *J Appl. Phys.* **34** (1963) 323

[3] Mullins W W. and Sekerka R.F , *J. Appl. Phys.* **35** (1964) 444

[4] Caroli B., Caroli C. and Roulet B., *J. Phys. (Paris)* **43** (1982) 1767.

[5] Oswald P., Bechhoefer J. and Libchaber A., *Phys Rev. Lett.* **58** (1987) 2318.

[6] Simon A J , Bechhoefer J. and Libchaber A., *Phys. Rev. Lett.* **61** (1988) 2574.

[7] Bechhoefer J., Simon A.J., Libchaber A. and Oswald P., *Phys. Rev. A* **40** (1989) 2042.

[8] Oswald P , Bechhoefer J., Libchaber A. and Lequeux F , *Phys. Rev. A* **36** (1987) 5832.

[9] Melo F. and Oswald P., *Phys Rev Lett.* **64** (1990) 1381.

[10] Cladis P.E., Gleeson J T , Finn P L. and Brand H.R., *Phys. Rev. Lett.* **67** (1991) 3239.

[11] Brand H.R. and Cladis P.E., *Phys. Rev Lett.* **72** (1994) 104.

[12] Cladis P.E., Slaney A J , Goodby J.W and Brand H.R , *Phys. Rev. Lett* **72** (1994) 226

[13] Grinfeld M.A., *Dokl Akad. Nauk. SSSR* **290** (1986) 1358 [*Sov Phys. Dokl* **31** (1987) 831]

[14] Balibar S., Edwards D.O. and Saam W.F., *J Low Temp Phys* **82** (1991) 119

[15] Bowley R.M. and Nozières P., *J. Phys. I France* **2** (1992) 433.

[16] Torii R.H. and Balibar S., *J. Low Temp. Phys* **89** (1992) 391.

[17] Yokoyama H , Kobayashi S. and Kamei H., *Mol. Cryst. Liq Cryst.* **129** (1985) 109

[18] de Gennes P-G., *Solid State Commun.* **8** (1970) 213.

[19] Herring C., *Phys. Rev.* **82** (1951) 87.

[20] Melo F. and Oswald P , *Ann Chim. Phys* **16** (1991) 237.

[21] Wulff G , *Z. Krist.* **34** (1901) 449.

[22] Nozières P., Solids Far From Equilibrium, C. Godrèche, Ed. (Aléa, Saclay, 1989)

[23] Galatola P., Fournier J B. and Durand G., *Phys. Rev. Lett.* **73** (1994) 2212.

[24] Fournier J.B., submitted.

[25] Landau L.D. and Lifschitz E.M , Statistical Physics, 3rd edition (Pergamon, Oxford, 1980).

[26] de Gennes P-G and Prost J., The Physics of Liquid Crystals (Academic Press, New York, 1993).

[27] Lavrentovich O.D., *Sov Phys JETP* **64**, (1986) 984

[28] Fournier J B., Dozov I. and Durand G., *Phys. Rev A* **41** (1990) 2252.

[29] Demus D. *et al.*, Flussige Kristalle in Tabellen (VEB, Liepzig, 1974).

[30] Young C.Y., Pindak R., Clark N A. and Meyer R B., *Phys. Rev Lett.* **40** (1978) 773.

[31] Pershan P S., Braslau A., Weiss A.H. and Als-Nielsen J., *Phys. Rev. A* **35** (1987) 4800.

[32] Fournier J.B and Durand G., *J Phys. II France* **1** (1991) 845

[33] Scheffer T.J., Gruler H. and Meier G., *Solid State Commun.* **11** (1972) 253.

[34] Meyer R.B. and Pershan P.S., *Solid State Commun.* **13** (1973) 989.

[35] Allet C., Kléman M. and Vidal P , *J. Phys. (Paris)* **39** (1978) 181

[36] Perez A., Brunet M. and Parodi O., *J. Phys. Lett. (Paris)* **20** (1978) L-353.

[37] Bouligand Y. and Kléman M., *J. Phys. (Paris)* **40** (1979) 79.

[38] Bourdon L., Sommeria J. and Kléman M., *J Phys. (Paris)* **43** (1982) 77.

[39] Friedel G. and Grandjean F., *Bull Soc. Fr. Mineral* **33** (1910) 409.

[40] Dubois-Violette E., *C.R. Acad. Sci.* **273** (1971) 923.

[41] Feng Q., Pesch W. and Kramer L., *Phys Rev. A* **45** (1992) 7242

[42] Fournier J.B , Warenghem M. and Durand G , *Phys Rev. E* **47** (1993) 1144